

Tunable amplification and cooling of a diamond resonator with a microscope

Harishankar Jayakumar,^{1,*} Behzad Khanaliloo,^{1,*} David P. Lake,¹ and Paul E. Barclay^{1,†}

¹*Institute for Quantum Science and Technology, University of Calgary, Calgary, AB, T2N 1N4, Canada*

(Dated: Compiled March 12, 2021)

Controlling the dynamics of mechanical resonators is central to quantum science and metrology applications. Optomechanical control of diamond resonators is attractive owing to diamond's excellent physical properties and its ability to host electronic spins that can be coherently coupled to mechanical motion. Using a confocal microscope, we demonstrate tunable amplification and damping of a diamond nanomechanical resonator's motion. Observation of both normal mode cooling from room temperature to 80K, and amplification into self-oscillations with 60 μ W of optical power is observed via waveguide optomechanical readout. This system is promising for quantum spin-optomechanics, as it is predicted to enable optical control of stress-spin coupling with rates of ~ 1 MHz (100 THz) to ground (excited) states of diamond nitrogen vacancy centers.

I. INTRODUCTION

The interaction between light and mechanical systems underlies breakthroughs in physics ranging from optical tweezers [1] to gravitational wave detection [2]. Nanoscale systems harnessing this interaction have led to advances in quantum nanomechanics [3–9], sensing [10–13], and nonlinear optics [14–18]. An essential ingredient to many of these demonstrations is dynamic optomechanical back action, which allows energy exchange between optical and mechanical domains [19, 20]. Controlling diamond nanomechanical systems via optomechanical back action is of growing interest, fueled by diamond's exceptional properties [21], and by demonstrations of diamond spin manipulation using piezoelectronically driven mechanical resonators [22–31]. Controlling resonator motion optomechanically provides a path towards photon-phonon-spin coupling and technologies ranging from spin-spin entanglement [32, 33] to quantum transduction [34]. Back action can also enhance the performance of diamond resonators used for sensing [35–37]. In this article, we show that optomechanical back action acting on modes of a diamond resonator vibrating in or out of plane can be selectively be created and controlled by adjusting the focal position of a microscope that commonly serves as an optical interface with diamond colour centres. Using this technique, we cool a diamond nanomechanical resonator, as well as amplify its motion sufficiently for mechanical control of diamond spins via their predicted coupling to phonons.

Optomechanical damping and amplification, for example by optical gradient [38], radiation pressure [4, 39, 40], or photothermal [36, 41–45] forces typically relies on feedback from a cavity [19, 20], waveguide coupler [45], or

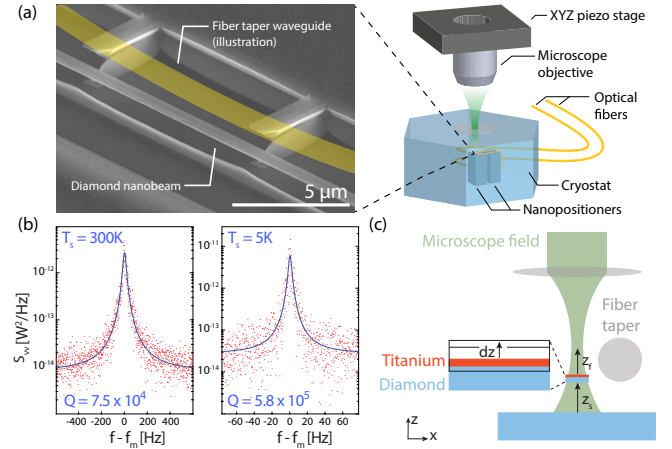


FIG. 1. (a) Schematic of the optomechanical system and apparatus. A microscope objective mounted on a piezo stage focuses a green laser onto the sample. The sample and fiber taper are located in a cryostat on nanopositioners. SEM image: a diamond nanobeam similar to that used in the experiment, with an illustration of the dimpled optical fiber taper drawn in yellow in approximately the position used for evanescent coupling to the nanobeam. Also visible are diamond supports used to stabilize the fiber taper during measurements. (b) Power spectral density of the fiber taper transmission near the v_1 nanobeam mode frequency at room and low temperature. (c) Schematic of the geometry of the optomechanical system.

external optoelectronics [46]. Inspired in part by optical tweezers, here we introduce a system that operates in an optical intensity gradient dominated regime of optomechanics and does not require a cavity or coupling to optical resonances [44]. The dynamic optomechanical back action is photothermal in nature, and is tuned through translation of a microscope focus, allowing both the strength and the sign of the optomechanical damping to be adjusted. This system, which adds confocal microscopy to our previously demonstrated waveguide optomechanical experiment [45], provides a combination of tunable optomechanical actuation and sensitive

* These authors contributed equally. Current address of HJ: University of Minnesota, 321 Church St SE, Minneapolis, MN 55455, harish@umn.edu; DL: California Institute of Technology, 1200 E California Blvd, Pasadena, CA 91125, United States; BK: Rockley Photonics Inc.

† pbarclay@ucalgary.ca

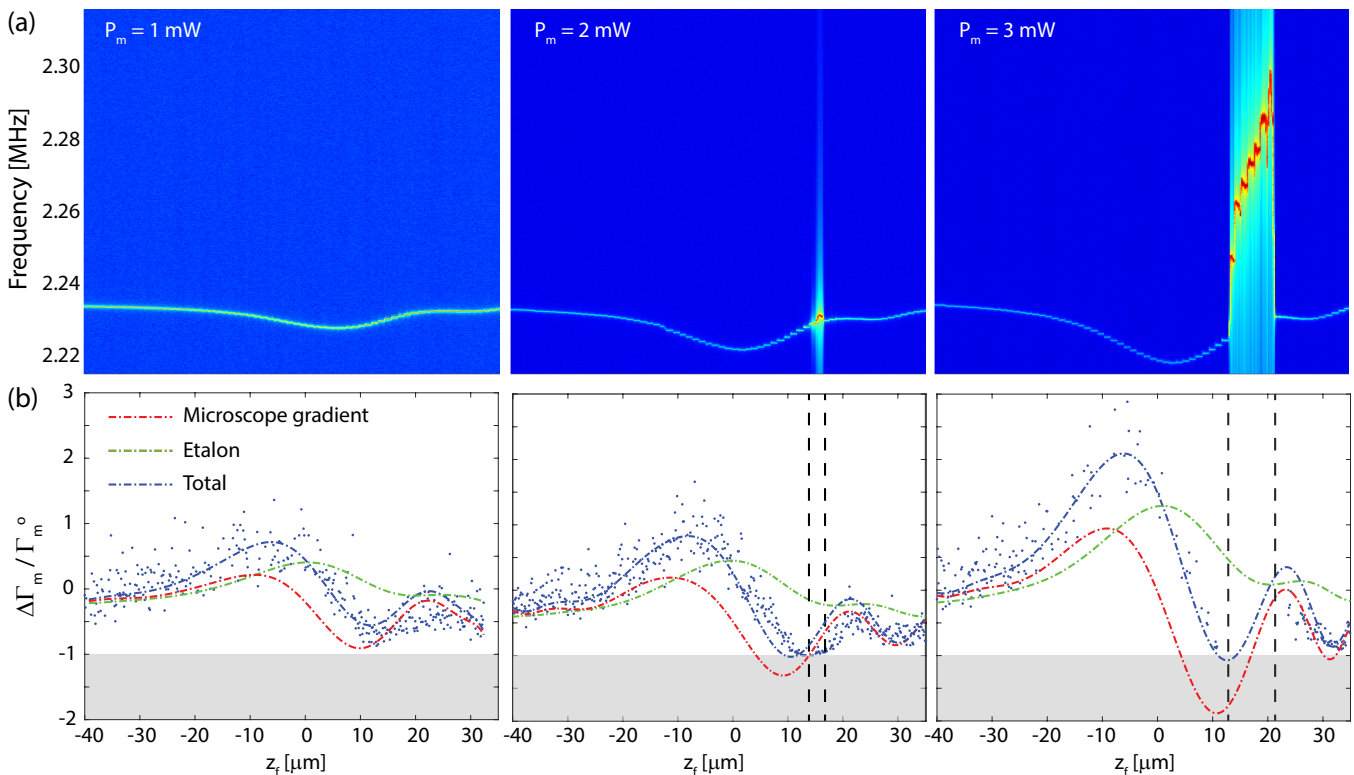


FIG. 2. (a) Spectrograph showing power spectral density of the \mathbf{v}_1 nanobeam mode as a function of microscope focus height, for varying green laser power. The sample is at room temperature. Negative z_f indicates that the focal position is below the nanobeam. (b) Optomechanical damping of \mathbf{v}_1 , normalized by its intrinsic dissipation rate, as a function of focal height and varying power. Fits are from the model in Eq. (1) input with a normalized $I(z_f)$ profile derived from Δf_m . Contributions from the etalon and microscope gradient terms in Eq. (2) are shown. Shaded regions indicate where optomechanical damping will cause self-oscillation.

optomechanical readout. It allows normal-mode cooling of a diamond mechanical resonator from room temperature to ~ 80 K, and excitation of nanomechanical self-oscillations whose stress field is predicted to allow control of nitrogen vacancy (NV) center spins [22]. These self-oscillations are observed for continuous wave excitation from a 532 nm laser with power as low as $60 \mu\text{W}$. Unlike previous demonstrations of photothermal backaction [36, 41–44], neither an external cavity nor a wavelength tunable laser is required to adjust the backaction between damping and anti-damping regimes. Furthermore, we leverage its sensitivity to the microscope field gradient to selectively excite vertical as well as horizontal modes of the nanobeam, the latter of which can be difficult to probe using conventional optical interferometry measurements of nanomechanical devices [47] as their motion primarily induces intensity rather than phase changes on reflected light.

II. DEVICE AND EXPERIMENTAL SETUP

The optomechanical system studied here, illustrated in Fig. 1(a), consists of a diamond nanobeam (dimensions $l \times w \times t = 50 \times 0.5 \times 0.25 \mu\text{m}^3$) illuminated by a green (532 nm) laser input to an objective (Sumitomo long working distance, 0.55 NA) mounted on a three-axis stage. The nanobeam is fabricated from single crystal diamond (Element Six, optical grade, $3 \times 3 \text{ mm}^2$ area, polished by Delaware Diamond Knives) using undercut etching [45], and its top surface is coated with titanium (~ 5 nm thickness, deposited using electron beam evaporation), which enhances photothermal effects discussed below. The nanobeam is suspended $\sim 2 \mu\text{m}$ above the diamond substrate, as shown in Fig. 1(a).

In the results presented below, we show that translating the microscope controls the dynamics of the nanobeam’s motion. These dynamics are monitored using an optical fiber taper waveguide (diameter $\sim 1 \mu\text{m}$) [48] evanescently coupled to the nanobeam, as illustrated in Fig. 1(a). The fiber taper and the diamond sample are mounted in a closed cycle cryostat (Montana Instruments) operating in high vacuum over temperatures

from 5K to 300K, and are aligned using nanopositioners (Attocube). Nanobeam motion is monitored with up to fm/ $\sqrt{\text{Hz}}$ sensitivity by detecting fluctuations in the coupling between the fiber taper and the nanobeam, as described in Ref. [45]. Nanobeam resonance dynamics are measured from the power spectral density S_{vv} of the photodetected transmission of a 1570 nm source through the fiber taper.

Characterization of the fundamental nanobeam vertical mechanical resonance (\mathbf{v}_1) in absence of the microscope field is shown in Fig. 1(b), which plots S_{vv} over the frequency (f) range spanning \mathbf{v}_1 resonance frequency f_m , in high vacuum ($< 10^{-5}$ Torr) at 300K and 5K operating temperatures. The peak in S_{vv} is thermally driven motion of \mathbf{v}_1 , whose dynamics are determined by dissipation rate $\Gamma_m = 2\pi f_m/Q_m$ where Q_m is mechanical quality factor. Fitting S_{vv} with a thermomechanical noise spectrum [49] we find $Q_m = 7.5 \times 10^4$ and 5.8×10^5 at 300K and 5K, respectively. The fiber taper input power is sufficiently low (a few μW) so that it does not affect the dynamics.

III. TUNABLE OPTOMECHANICAL BACKACTION

Turning on the microscope field introduces optomechanical back action that can be analyzed using the geometry in Fig. 1(c). The field intensity I in the nanobeam depends on both the nanobeam's height above the substrate, z_s , and its distance to the microscope focal plane, z_f , and can be approximated as $I = I_f(z_f)\chi(z_s)$. Here I_f describes the z_f dependence of I . The etalon enhancement factor $\chi(z_s)$ describes interference between reflections from the etched diamond surface below the nanobeam, the titanium coated nanobeam, and the incident field, which will combine to create a standing wave pattern. In this simplified model $I_f(z_f)$ implicitly accounts for geometry related local field corrections, for example local optical resonances of the nanobeam and the effect of the titanium layer, and we have assumed that changes in z_s from nanobeam motion are sufficiently small that the etalon contribution can be treated as a separable scaling factor. Vertical nanobeam displacement dz modifies z_s and z_f by $\pm dz$, respectively, which in turn changes I . This optomechanical feedback, when combined with a lag between the nanobeam position and forces proportional to I , amplifies or damps mechanical motion.

The dominant optical microscope forces on the nanobeam were found to be photothermal [36, 42], whose optomechanical damping $\Delta\Gamma_m$ is given by

$$\frac{\Delta\Gamma_m(z_f)}{\Gamma_m^o} = Q_m^o \frac{2\pi f_m^o \tau}{1 + (2\pi f_m(z_f)\tau)^2} \mathcal{G} \frac{dI}{dz} \sigma, \quad (1)$$

where f_m^o , Γ_m^o and Q_m^o are intrinsic values in absence of the microscope field. This model follows and modifies

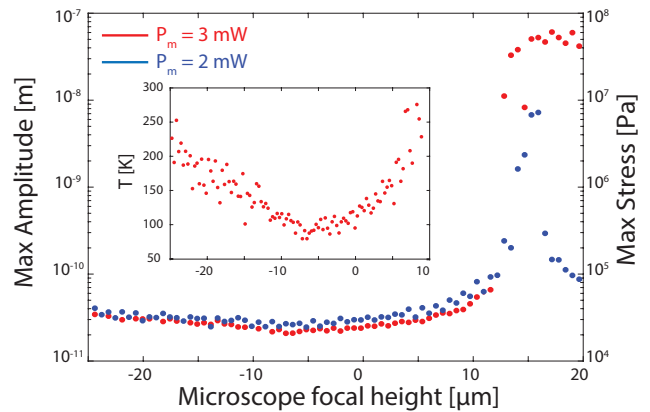


FIG. 3. Amplitude (left axis) and maximum internal dynamic stress (right axis) of the \mathbf{v}_1 mode at room temperature as a function of microscope focal plane height for 2 mW and 3 mW microscope power. The sample is at room temperature. When the nanobeam self oscillates, maximum stress just below ~ 100 MPa near the nanobeam clamping points can be realized. Inset: Effective normal mode temperature for 3 mW microscope power as a function of microscope height scanning through the regime of maximum damping.

that previously analyzed in [45] in absence of a microscope field. Unlike in [45], the field from the fiber taper does not sufficiently heat the nanobeam to induce any backaction. Instead, the nanobeam is deflected by power absorbed from the microscope field. The nanobeam deflection for absorbed power σI is determined by photothermal coupling coefficient \mathcal{G} (units of m/W), and depends on the nanobeam's geometry and internal compressive stress [45]. The titanium layer increases absorption cross-section σ , but is not generally necessary to observe dynamic back action [45]. A non-instantaneous thermal response time τ is required for optomechanical heating or cooling. Finite element (COMSOL) simulations predict $2\pi f_m \tau \sim 3$, accounting for the reduced thermal conductivity of nanostructured diamond [50].

The gradient of the microscope intensity plays a critical role in determining whether dI/dz , and as a result $\Delta\Gamma_m$, is positive or negative. This is in contrast to cavity optomechanics, where back action is dominated by χ whose sign is independent of external optics. To study the microscope back action, the objective was aligned with the center of the nanobeam and scanned vertically (1 μm steps, 2.9 s/step) while monitoring S_{vv} . Figure 2(a) shows this measurement at room temperature for microscope powers $P_m = 1, 2$ and 3 mW. The mechanical frequency $f_m(z_f) = f_m^o + \Delta f_m(z_f)$ decreases as the microscope is focused on the nanobeam, consistent with optical heating of a compressively stressed device [45]. Δf_m follows a profile reminiscent of the microscope laser intensity's z_f dependence, providing a measure of the $I_f(z_f)$ profile that can be input to the model in Eq. (1), as discussed below. The asymmetry and oscillations in

$\Delta f_m(z_f)$ are related to aberrations from the cryostat window [51]. In general, Δf_m is also affected by dynamic photothermal, and dynamic and static optical gradient force effects. However, they are predicted to be smaller than the observed $|\Delta f_m|$ [45].

The influence of the microscope on the nanobeam dynamics is revealed dramatically in Fig. 2(a) near $z_f = 15 \mu\text{m}$, where for $P_m = 2$ and 3 mW the peak value of S_{vv} increases, indicating nanomechanical self-oscillation, and f_m shifts due to nonlinear nanomechanical effects related to large amplitude motion [45]. To analyze this quantitatively, the measured $\Delta\Gamma_m(z_f)$ is plotted in Fig. 2(b), showing that motion is either damped ($\Delta\Gamma_m > 0$) or amplified ($\Delta\Gamma_m < 0$) depending on the microscope focus: the sign of $\Delta\Gamma_m$ changes as the focus is scanned from above to below the nanobeam. Near $z_f = 15 \mu\text{m}$, $\Gamma_m \sim 0$, the nanobeam enters a regime of self-oscillation, in agreement with the increase in S_{vv} peak amplitude.

This behavior illustrates a key feature of this system: the dependence of the sign of $\Delta\Gamma_m(z_f)$ on the microscope intensity gradient. By fitting the data in Figs. 2(b) with the model from Eq. (1), the relative contribution from the microscope gradient and the etalon were extracted. This requires expanding the intensity gradient,

$$\frac{dI}{dz} = -\chi \left(\frac{dI_f(z_f)}{dz_f} - I_f(z_f) \frac{1}{\chi} \frac{d\chi}{dz_s} \right), \quad (2)$$

and inferring dI_f/dz_f and $I_f(z_f)$ from $\Delta f_m(z_f)$ to within a proportionality constant. In addition to this constant, the fit requires a fitting parameter $\propto \chi$ that governs the relative contributions of the intensity gradient and the etalon terms in Eq. (2). Contributions from these two terms are shown in Fig. 2(b), showing that in our experiment the microscope gradient is the dominant factor while the smaller etalon contribution damps mechanical motion and shifts the zero of $\Delta\Gamma_m(z_f)$. The imperfect fits reveal the approximate nature of the model. For example, it is possible that the microscope position and the etalon response, which in general is a standing wave pattern, are not entirely separable. In future, detailed numerical simulations of the microscope field and its interaction with the nanobeam and the surrounding diamond structure would provide additional insight into optimization of the strength of the gradient contribution and minimization of the etalon contribution.

The amplification and damping is further analyzed in Fig. 3, which plots the RMS amplitude for varying z_f and P_m , extracted from the area under S_{vv} normalized by the thermomechanical vibration amplitude in absence of the microscope field [52]. When $P_m = 3$ mW, the self-oscillations reach close to 100 nm, three orders of magnitude greater than the nanobeam's intrinsic thermal motion. In contrast, when the microscope position is set to $z_f \sim -5 \mu\text{m}$, the thermal motion of the nanobeam is damped, cooling the resonance to $T_{\text{eff}} \sim 80$ K from the sample temperature $T_s = 300$ K, as shown in the inset to Fig. 3. This inference of temperature from resonance area was found to be consistent with $T_{\text{eff}} = T_s / (1 + \Delta\Gamma_m / \Gamma_m^o)$

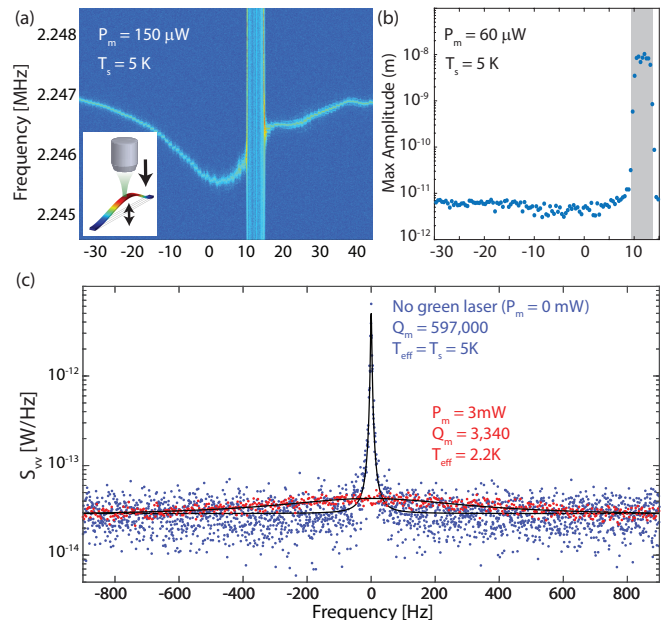


FIG. 4. Nanobeam-microscope optomechanics at cryogenic temperature $T_s = 5$ K: (a) Spectrograph and (b) oscillation amplitude of the \mathbf{v}_1 nanobeam mode motion for varying focal plane height, detected via fiber taper transmission. (c) Power spectral density of the fiber taper transmission detected \mathbf{v}_1 mode motion with the microscope off ($P_m = 0$ mW) and on ($P_m = 3$ mW) with z_f optimized to maximize $\Delta\Gamma_m$.

predicted from $\Delta\Gamma_m$ in Fig. 2(b) [20].

IV. CRYOGENIC OPERATION

A. Low power self-oscillations and cooling

The impact of back action is increased in cryogenic conditions where the intrinsic mechanical dissipation of the diamond resonator is reduced. The improvement in device performance at low temperature is illustrated in Fig. 1(b), which shows that Q_m^o increases by an order of magnitude when the sample temperature is lowered from 300 K to 5 K. As a result, for a given optomechanical backaction $|\Delta\Gamma_m|$, which is nominally independent of temperature and Q_m^o , the relative change in mechanical dissipation, $|\Delta\Gamma_m / \Gamma_m^o| \propto Q_m^o$, increases. This lowers the power required for optomechanical self-oscillation ($\Delta\Gamma_m / \Gamma_m^o = -1$) or cooling to a desired T_{eff} .

Figures 4(a) and 4(b) illustrate this effect by showing S_{vv} and the mechanical vibration amplitude, respectively, at $T_s = 5$ K, for varying z_f . In these measurements the microscope power was reduced to $P_m = 150 \mu\text{W}$ and $60 \mu\text{W}$, respectively. Despite the order of magnitude lower P_m compared to the room temperature measurements in Figs. 2 and 3, self-oscillations with comparable amplitude are observed.

A tantalizing prospect given the nanobeam's increase in Q_m^o at cryogenic temperature is optomechanical cooling: for the \mathbf{v}_1 mode $T_{\text{eff}} \approx 0.3$ K is naively expected at $T_s = 5$ K from the $\Delta\Gamma_m$ observed at room temperature in Fig. 2(b). Figure 4(c) compares S_{vv} of this mode at $T_{\text{eff}} = 5$ K with and without the 3 mW microscope field turned on. With the field on and the focus optimized to maximize damping, $Q_m \sim 3340$ is inferred from the resonance linewidth. Although this is a two orders of magnitude increase in linewidth, the corresponding measured area under S_{vv} was only reduced by a factor of 2.4 by the microscope field, resulting in $T_{\text{eff}} = 2.2$ K.

The discrepancy between the large broadening of the resonance and the comparatively modest change in T_{eff} can arise from several sources. At $T_s = 5$ K the specific heat of diamond is four orders of magnitude smaller than at room temperature. As a result, the microscope field can more easily increase the bath temperature of the nanobeam, counteracting cooling via optomechanical damping. Additional linewidth broadening could arise from fluctuations of the mechanical resonance frequency induced by the microscope field. Comparing the resonance linewidth for $P_m = 3$ mW at $T_s = 5$ K in Fig. 4(c) with the corresponding maximum room temperature linewidth in Fig. 2(b), we see infer $\Delta\Gamma_m|_{5\text{K}}/\Delta\Gamma_m|_{300\text{K}} \sim 5$ if damping rate is assumed to be proportional to the linewidth. Such an enhancement in damping at low temperature requires that photothermal coupling increases in cryogenic conditions, for example due to changes in the nanobeam's compressive stress [45]. However, measurements discussed below reveal that other mechanisms can contribute significantly to linewidth broadening at cryogenic temperatures.

B. In-plane mode excitation and line broadening

The device's higher Q_m^o at cryogenic temperatures also enabled excitation of in-plane nanobeam motion. This is shown in Fig. 5, which plots S_{vv} of the in-plane fundamental \mathbf{h}_1 resonance near $f_m = 3.0$ MHz as a function of lateral (x) displacement of the objective for $P_m = 450 \mu\text{W}$. The $4 \mu\text{m}$ x scan length is smaller than the z scans owing to the microscope's tight lateral focus in comparison to its depth of focus. Self-oscillation occurs near $x = 0.75 \mu\text{m}$, while for negative x damping is observed. This asymmetric optomechanical response indicates that the nanobeam deflects laterally in a fixed direction when heated, independent of whether the focus is on the right or left side of the nanobeam.

Further analysis of the dependence of the \mathbf{h}_1 resonance dynamics on the microscope field confirm that mechanisms in addition to optomechanical backaction broaden the mechanical lineshape. Figure 6(a) plots the resonance area ($\propto T_{\text{eff}}$) for varying microscope displacement along x with $P_m \sim 200 \mu\text{W}$ set below the threshold for self-oscillation. This clearly illustrates the asymmetric response of the optomechanical damping as a function

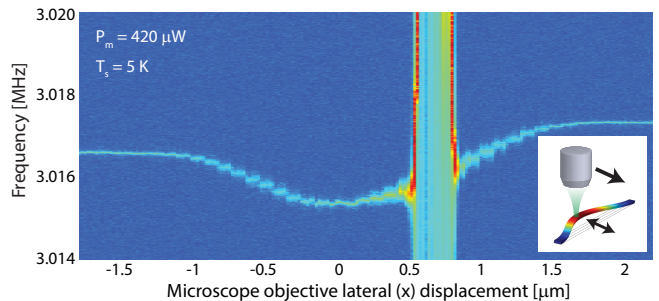


FIG. 5. Exciting in-plane motion: Spectrograph of the fundamental in-plane \mathbf{h}_1 nanobeam mode motion for varying lateral focal spot position, detected via fiber taper transmission. $P_m = 420 \mu\text{W}$ and $T_s = 5$ K.

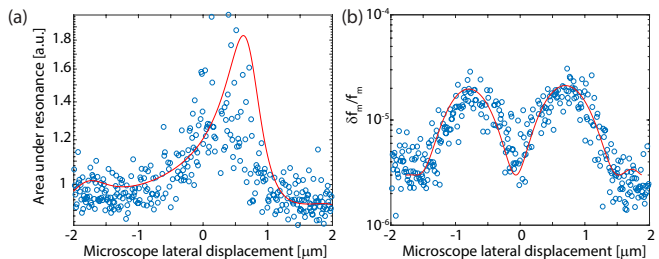


FIG. 6. Competition between optomechanical backaction and thermomechanical linewidth broadening. (a) Area under the \mathbf{h}_1 nanobeam mode spectrum for varying lateral focal spot position. (b) Corresponding linewidth extracted by fits to the mode spectrum. Measurements at $P_m = 200 \mu\text{W}$ and $T_s = 5$ K.

of x , and is consistent with the self-oscillation data in Fig. 5. In contrast, the measured linewidth, plotted in Fig. 6(b), varies symmetrically with x . Broadening is maximized when the nanobeam is positioned adjacent to the microscope focus, where the lateral gradient of the microscope field intensity is strong. This broadening occurs even when the nanobeam motion is being amplified. These observations suggest that displacements of the nanobeam relative to the microscope focus are causing spectral diffusion of f_m .

To better understand the dependence of the mode area (A) and the measured linewidth (δf) on microscope position, we fit the x dependent data in Fig. 6 with:

$$A(x) = A_0 \left[1 + \alpha_1 \frac{I(x)}{1 + \beta \frac{dI}{dx}} \right], \quad (3)$$

$$\delta f(x) = \delta f_o \left[1 + \alpha_2 \frac{dI}{dx} \right], \quad (4)$$

where fitting parameter α_1 describes the increase in T_s from the microscope field, and parameter β describes the strength of the photothermal optomechanical backaction and its effect on $\Delta\Gamma$. Fitting parameter α_2 describes a contribution to spectral broadening resulting from the

nanobeam's overlap with the gradient of the microscope field intensity, for example that manifest due to variations in the position of the focal spot relative to the nanobeam. The fits in Fig. 6 are created by assuming that $I(x)$ is directly proportional to the measured $\Delta f_m(x)$, similar to the room temperature analysis in Fig. 2(b).

This model has good agreement with the data, and confirms that in addition to optomechanical damping, the linewidth is being broadened by additional mechanisms described here phenomenologically by non-zero α_2 . Further investigation into the source of this broadening is required. For example, measurements of the Allan variance of the mechanical frequency will reveal the timescale over which it is fluctuating and give insight into the nature of any technical noise affecting it. Time domain measurements of mechanical ring-down will provide a direct measurement of Γ_m . Together with power dependent measurements of δf_m , this may allow improvement of the efficiency of the photothermal cooling process in cryogenic conditions.

Note that T_{eff} inferred from the area of S_{vv} is unaffected by spectral diffusion [53], and that at room temperature we observe close agreement between T_{eff} extracted from A and δf_m , respectively. This indicates that the spectral broadening by the microscope is specific to the cryogenic measurements reported here.

V. DISCUSSION

This system's potential for spin-optomechanics is significant. Confocal microscopes are used for diamond spin spectroscopy, making this approach suited for controlling

coupling of phonons and spins. For the self-oscillations reported here, dynamic stress fields of ~ 100 MPa are predicted (COMSOL), as shown in Fig. 3. This corresponds to a spin-stress coupling rate $G_g/2\pi \sim 1$ MHz and $G_e/2\pi \sim 100$ THz, for the ground and excited states, respectively, of a negatively charged NV, which are comparable to coupling rates in piezo-based stress manipulation experiments [22]. Optomechanical spin control will provide a path towards creating a quantum transducer [30, 34] for coupling photons to spins without direct optical color center transitions, enabling interfacing telecommunication photons with spin quantum memories [54].

In conclusion, we have demonstrated optomechanical control of a diamond resonator using a microscope. To the best of our knowledge, this is the first demonstration of tunable optomechanical damping and amplification of a nanomechanical resonator without a cavity, etalon, or other external feedback component. Using this tunable optomechanical damping, we have cooled the nanobeam's fundamental mode to below 80K, and amplified its motion sufficiently for spin-phonon coupling at rates that exceed relevant spin decoherence rates [22, 54]. We have also studied the interplay between the nanomechanical resonator of the microscope field at low temperature, providing a jumping off point for future studies of photothermal cooling in cryogenic environments.

ACKNOWLEDGMENTS

Thank you to Aaron Hryciw, J.P. Hadden and M. Mitchell for assistance. This work was supported by NSERC (Discovery and Research Tools and Instruments), CFI, AITF and NRC.

-
- [1] A. Ashkin, Acceleration and trapping of particles by radiation pressure, *Phys. Rev. Lett.* **24**, 156 (1970).
 - [2] L. Scientific, B. Abbott, R. Abbott, T. Abbott, F. Acernese, K. Ackley, C. Adams, T. Adams, P. Addesso, R. Adhikari, *et al.*, Gw170104: observation of a 50-solar-mass binary black hole coalescence at redshift 0.2, *Physical Review Letters* **118**, 221101 (2017).
 - [3] S. Gröblacher, K. Hammerer, M. R. Vanner, and M. Aspelmeyer, Observation of strong coupling between a micromechanical resonator and an optical cavity field, *Nature* **460**, 724 (2009).
 - [4] J. Chan, T. P. M. Alegre, A. H. Safavi-Naeini, J. T. Hill, A. Krause, S. Groblacher, M. Aspelmeyer, and O. Painter, Laser cooling of a nanomechanical oscillator into its quantum ground state, *Nature* **478**, 89 (2011).
 - [5] J. D. Cohen, S. M. Meenehan, G. S. MacCabe, S. Gröblacher, A. H. Safavi-Naeini, F. Marsili, M. D. Shaw, and O. Painter, Phonon counting and intensity interferometry of a nanomechanical resonator, *Nature* **520**, 522 (2015).
 - [6] R. Riedinger, S. Hong, R. A. Norte, J. A. Slater, J. Shang, A. G. Krause, V. Anant, M. Aspelmeyer, and S. Gröblacher, Non-classical correlations between single photons and phonons from a mechanical oscillator, *Nature* **530**, 313 (2016).
 - [7] V. Sudhir, R. Schilling, S. A. Fedorov, H. Schütz, D. J. Wilson, and T. J. Kippenberg, Quantum correlations of light from a room-temperature mechanical oscillator, *Phys. Rev. X* **7**, 031055 (2017).
 - [8] T. P. Purdy, K. E. Grutter, K. Srinivasan, and J. M. Taylor, Quantum correlations from a room-temperature optomechanical cavity, *Science* **356**, 1265 (2017).
 - [9] R. Riedinger, A. Wallucks, I. Marinković, C. Löschnauer, M. Aspelmeyer, S. Hong, and S. Gröblacher, Remote quantum entanglement between two micromechanical oscillators, *Nature* **556**, 473 (2018).
 - [10] G. Anetsberger, E. Gavartin, O. Arcizet, Q. Unterreithmeier, E. Weig, M. Gorodetsky, J. Kotthaus, and T. Kippenberg, Measuring nanomechanical motion with an imprecision below standard quantum limit, *Phys. Rev. A* **82**, 061804 (2010).
 - [11] E. Gavartin, P. Verlot, and T. Kippenberg, A hybrid on-

- chip optomechanical transducer for ultrasensitive force measurements, *Nature Nanotech.* **7**, 509 (2012).
- [12] S. Forstner, S. Prams, J. Knittel, E. van Ooijen, J. Swaim, G. Harris, A. Szorkovszky, W. Bowen, and H. Rubinsztein-Dunlop, Cavity optomechanical magnetometer, *Phys. Rev. Lett.* **108**, 120801 (2012).
- [13] M. Wu, N. L.-Y. Wu, T. Firdous, F. F. Sani, J. E. Losby, M. R. Freeman, and P. E. Barclay, Nanocavity optomechanical torque magnetometry and radiofrequency susceptometry, *Nature Nanotechnology* **12**, 127 (2017).
- [14] A. H. Safavi-Naeini, T. M. Alegre, J. Chan, M. Eichenfield, M. Winger, Q. Lin, J. T. Hill, D. Chang, and O. Painter, Electromagnetically induced transparency and slow light with optomechanics, *Nature* **472**, 69 (2011).
- [15] S. Weis, R. Rivière, S. Deléglise, E. Gavartin, O. Arcizet, A. Schliesser, and T. J. Kippenberg, Optomechanically induced transparency, *Science* **330**, 1520 (2010).
- [16] C. Dong, V. Fiore, M. C. Kuzyk, and H. Wang, Optomechanical dark mode, *Science* **338**, 1609 (2012).
- [17] Y. Liu, M. Davanço, V. Aksyuk, and K. Srinivasan, Electromagnetically induced transparency and wideband wavelength conversion in silicon nitride microdisk optomechanical resonators, *Phys. Rev. Lett.* **110**, 223603 (2013).
- [18] D. P. Lake, M. Mitchell, Y. Kamaliddin, and P. E. Barclay, Optomechanically induced transparency and cooling in thermally stable diamond microcavities, *ACS Photonics* **5**, 782 (2018).
- [19] T. Kippenberg and K. Vahala, Cavity optomechanics: Back-action at the mesoscale, *Science* **321**, 1172 (2008).
- [20] M. Aspelmeyer, T. J. Kippenberg, and F. Marquardt, Cavity optomechanics, *Rev. Mod. Phys.* **86**, 1391 (2014).
- [21] I. Aharonovich, A. D. Greentree, and S. Prawer, Diamond photonics, *Nature Photon.* **5**, 397 (2011).
- [22] D. Lee, K. W. Lee, J. V. Cady, P. Ouartchaiyapong, and A. C. B. Jayich, Topical review: spins and mechanics in diamond, *Journal of Optics* **19**, 033001 (2017).
- [23] E. R. MacQuarrie, T. A. Gosavi, N. R. Jungwirth, S. A. Bhave, and G. D. Fuchs, Mechanical spin control of nitrogen-vacancy centers in diamond, *Phys. Rev. Lett.* **111**, 227602 (2013).
- [24] P. Ouartchaiyapong, K. W. Lee, B. A. Myers, and A. C. B. Jayich, Dynamic strain-mediated coupling of a single diamond spin to a mechanical resonator, *Nat. Commun.* **5**, 4429 (2014).
- [25] J. Teissier, A. Barfuss, P. Appel, E. Neu, and P. Maletinsky, Strain coupling of a nitrogen-vacancy center spin to a diamond mechanical oscillator, *Phys. Rev. Lett.* **113**, 020503 (2014).
- [26] A. Barfuss, J. Teissier, E. Neu, A. Nunnenkamp, and P. Maletinsky, Strong mechanical driving of a single electron spin, *Nature Phys.* **11**, 820 (2015).
- [27] E. R. MacQuarrie, T. A. Gosavi, A. M. Moehle, N. R. Jungwirth, S. A. Bhave, and G. D. Fuchs, Coherent control of a nitrogen-vacancy center spin ensemble with a diamond mechanical resonator, *Optica* **2**, 233 (2015).
- [28] S. Meesala, Y.-I. Sohn, H. A. Atikian, S. Kim, M. J. Burek, J. T. Choy, and M. Lončar, Enhanced strain coupling of nitrogen-vacancy spins to nanoscale diamond cantilevers, *Phys. Rev. Applied* **5**, 034010 (2016).
- [29] D. A. Golter, T. Oo, M. Amezcua, I. Lekavicius, K. A. Stewart, and H. Wang, Coupling a surface acoustic wave to an electron spin in diamond via a dark state, *Phys. Rev. X* **6**, 041060 (2016).
- [30] D. A. Golter, T. Oo, M. Amezcua, K. A. Stewart, and H. Wang, Optomechanical quantum control of a nitrogen-vacancy center in diamond, *Phys. Rev. Lett.* **116**, 143602 (2016).
- [31] S. Maity, L. Shao, S. Bogdanović, S. Meesala, Y.-I. Sohn, N. Sinclair, B. Pingault, M. Chalupnik, C. Chia, L. Zheng, *et al.*, Coherent acoustic control of a single silicon vacancy spin in diamond, *arXiv preprint arXiv:1910.09710* (2019).
- [32] M.-A. Lemonde, S. Meesala, A. Sipahigil, M. J. A. Schuetz, M. D. Lukin, M. Loncar, and P. Rabl, Phonon networks with silicon-vacancy centers in diamond waveguides, *Phys. Rev. Lett.* **120**, 213603 (2018).
- [33] M. C. Kuzyk and H. Wang, Phononic quantum networks of solid-state spins with alternating and frequency-selective waveguides, *arXiv preprint arXiv:1804.07862* (2018).
- [34] M. J. A. Schuetz, E. M. Kessler, G. Giedke, L. M. K. Vandersypen, M. D. Lukin, and J. I. Cirac, Universal quantum transducers based on surface acoustic waves, *Phys. Rev. X* **5**, 031031 (2015).
- [35] D. Rugar and P. Grütter, Mechanical parametric amplification and thermomechanical noise squeezing, *Phys. Rev. Lett.* **67**, 699 (1991).
- [36] R. A. Barton, I. R. Storch, V. P. Adiga, R. Sakakibara, B. R. Cipriany, B. Ilic, S. P. Wang, P. Ong, P. L. McEuen, J. M. Parpia, *et al.*, Photothermal self-oscillation and laser cooling of graphene optomechanical systems, *Nano Lett.* **12**, 4681 (2012).
- [37] Z. Yie, K. Turner, N. Miller, and S. Shaw, Sensitivity enhancement using parametric amplification in a resonant sensing array, in *Proceedings of the 13th Hilton Head Solid State Sensors and Actuators Conference* (2010).
- [38] Q. Lin, J. Rosenberg, X. Jiang, K. J. Vahala, and O. Painter, Mechanical oscillation and cooling actuated by the optical gradient force, *Phys. Rev. Lett.* **103**, 103601 (2009).
- [39] O. Arcizet, P. F. Cohadon, T. Briant, M. Pinard, and A. Heidmann, Radiation-pressure cooling and optomechanical instability of a micromirror, *Nature* **444**, 71 (2006).
- [40] S. Gigan, H. R. Böhm, M. Paternostro, F. Blaser, G. Langer, J. B. Hertzberg, K. C. Schwab, D. Bäuerle, M. Aspelmeyer, and A. Zeilinger, Self-cooling of a micromirror by radiation pressure, *Nature* **444**, 67 (2006), [arXiv:quant-ph/0607068](https://arxiv.org/abs/quant-ph/0607068).
- [41] C. Metzger, I. Favero, A. Ortlieb, and K. Karrai, Optical self cooling of a deformable fabry-perot cavity in the classical limit, *Phys. Rev. B* **78**, 035309 (2008).
- [42] C. H. Metzger and K. Karrai, Cavity cooling of a microlever, *Nature* **432**, 1002 (2004).
- [43] I. Favero, C. Metzger, S. Camerer, D. König, H. Lorenz, J. P. Kotthaus, and K. Karrai, Optical cooling of a micromirror of wavelength size, *Appl. Phys. Lett.* **90**, 104101 (2007).
- [44] D. Ramos, E. Gil-Santos, V. Pini, J. M. Llorens, M. Fernandez-Regulez, A. S. Paulo, M. Calleja, and J. Tamayo, Optomechanics with silicon nanowires by harnessing confined electromagnetic modes, *Nano Letters* **12**, 932 (2012), PMID: 22268657, <http://dx.doi.org/10.1021/nl204002u>.
- [45] B. Khanaliloo, H. Jayakumar, A. C. Hryciw, D. P. Lake, H. Kaviani, and P. E. Barclay, Single-crystal diamond

- nanobeam waveguide optomechanics, *Phys. Rev. X* **5**, 041051 (2015).
- [46] M. Poggio, C. Degen, H. Mamin, and D. Rugar, Feedback cooling of a cantilever's fundamental mode below 5 mk, *Physical Review Letters* **99**, 017201 (2007).
- [47] M. J. Burek, D. Ramos, P. Patel, I. W. Frank, and M. Lončar, Nanomechanical resonant structures in single-crystal diamond, *Appl. Phys. Lett.* **103**, 131904 (2013).
- [48] C. P. Michael, M. Borselli, T. J. Johnson, C. Chrystala, and O. Painter, An optical fiber-taper probe for wafer-scale microphotonic device characterization, *Opt. Express* **15**, 4745 (2007).
- [49] A. Cleland and M. Roukes, Noise processes in nanomechanical resonators, *J. Appl. Phys.* **92**, 2758 (2002).
- [50] W. Li, N. Mingo, L. Lindsay, D. A. Broido, D. A. Stewart, and N. A. Katcho, Thermal conductivity of diamond nanowires from first principles, *Phys. Rev. B* **85**, 195436 (2012).
- [51] M. J. Nasse and J. C. Woehl, Realistic modeling of the illumination point spread function in confocal scanning optical microscopy, *Josa a* **27**, 295 (2010).
- [52] M. Mitchell, B. Khanaliloo, D. P. Lake, T. Masuda, J. P. Hadden, and P. E. Barclay, Single-crystal diamond low-dissipation cavity optomechanics, *Optica* **3**, 963 (2016).
- [53] J. Moser, A. Eichler, J. Güttinger, M. I. Dykman, and A. Bachtold, Nanotube mechanical resonators with quality factors of up to 5 million, *Nature nanotechnology* **9**, 1007 (2014).
- [54] P. K. Shandilya, D. P. Lake, M. J. Mitchell, D. D. Sukachev, and P. E. Barclay, Optomechanical interface between telecom photons and spin quantum memory (2021), arXiv:2102.04597 [quant-ph].